Heritage Science

COMMENT

Open Access

# Corrosion mechanisms for lead-glazed pottery from Qibi Ming Tomb of the Tang Dynasty in Xianyang, China

Yanli Li[1], Panpan Liu[1], Yujia Luo[1], Mantang Ge[1], Huiping Xing[1*] and Yuhu Li[1*]

**Abstract**

Six corroded glazed pottery figurines, which excavated from the Qibi Ming Tomb of the Tang Dynasty in Xianyang, were selected to study the corrosion mechanism. Optical microscopy (OM), scanning electron microscopy equipped with energy dispersive X-ray spectrometry (SEM–EDS), Energy X-ray fluorescence spectrometry (EDX), and micro-Raman spectroscopy were applied to analyze the pristine composition of the glaze layer and pottery substrate, the composition and microstructure of corrosion products. The results indicate that lead-glazed pottery figurines are low-temperature PbO-CaO-$SiO_2$ glaze, with Pb as the main flux, and Cu, Fe as the main colorant. The corrosion products include $PbCO_3$, $CaCO_3$, $PbCO_3$·$PbCl_2$, $PbCl_2$, $PbO_2$, and Si-rich layer. There are *Aspergillus niger* and *Aspergillus sclerotiorum* on the surface of glazed pottery. These microorganisms produce organic acids and mold spots on the surface of the pottery figurines, which in turn cause corrosion pits to form on the surface of the figurines. Chemical corrosion reactions mainly include dissolution–precipitation, combination reaction, and oxidation reaction. This article describes the corrosion process of lead-glazed pottery figurines and establishes corresponding corrosion models. This study provides new insights into the corrosion mechanism of lead-glazed pottery, which is of great significance for studying pottery corrosion.

**Keywords** Lead-glazed pottery, Corrosion mechanism, Silver glaze, Oxidation reaction, Microorganism

## Introduction

In China, lead-glazed pottery technology appeared as early as the Warring States Period (475–221 B.C.) [1, 2]. Lead-glazed pottery was a low-temperature pottery that uses lead (Pb) as a flux and metal oxides as colorants. These glazes were green, yellow, brown, and black, with green glazes using copper oxide as colorants being the most popular [3]. With bright appearance and diverse shapes, this kind of glazed pottery has high artistic value, and occupies a very important position in the history of Chinese ceramics.

Lead oxide (PbO) was introduced into glazed pottery as a low melting point flux. The high polarization of $Pb^{2+}$ caused electrons to move away from oxygen in silicates, thereby reducing the temperature of Si–O bond breakage [4]. Glaze is a glass phase layer that covers the ceramic matrix and has properties similar to glass [5]. Glaze can enhance the aesthetics of objects, and more importantly, its dense texture can increase the mechanical strength of the pottery substrate and provide protection for the pottery substrate. However, after being buried for hundreds or even thousands of years, the chemical stability and hardness of the lead-glaze on the surface of glazed pottery were diminished, the bond between the pottery substrate and glaze was not firm, and various corrosion diseases were prone to occur [6–8]. The presence

*Correspondence:
Huiping Xing
xhp@snnu.edu.cn
Yuhu Li
liyuhu@snnu.edu.cn
[1] Engineering Research Center of Historical Cultural Heritage Conservation, Ministry of Education, School of Materials Science and Engineering, Shaanxi Normal University, Xi'an 710119, China

of corrosions on glazed pottery presents a significant risk to its preservation. Consequently, the investigation of the causes of corrosion in glazed pottery is of paramount importance. Such research can offer insights into the optimal preservation practices for unearthed glazed pottery, deepen comprehension of the corrosion processes affecting glazed pottery in natural settings, and establish a sound foundation for the selection of suitable protective and remedial measures. At present, there is a lack of systematic and comprehensive research on the corrosion mechanism of ancient Chinese glazed pottery. This article takes the glazed pottery excavated from the Qibi Ming Tomb of the Tang Dynasty as an example to study the physical and chemical corrosion process of glazed pottery, and the corrosion mechanism of microorganisms on glazed pottery, aiming to comprehensively explore the corrosion process and influencing factors of glazed pottery.

Qibi Ming was a famous ethnic minority general in the early Tang Dynasty. He was buried about 400 m north of Yaowangdong in Weicheng District, Xianyang City, Shaanxi Province. The tomb began excavation in 1973. More than 700 pieces of tricolor vessels, pottery figurines, and other burial objects were excavated from the tomb, which are of high value [9–11]. The excavated lead-glazed pottery figurines carry important historical and cultural information, which are of great significance for studying cultural exchange, ethnic exchange, and integration in the central and western regions. They provide important physical examples for the study of the composition and production technology of pottery artifacts during this historical period. The glaze layer on the surface of some lead-glazed pottery figurines has partially or completely peeled off, and the pottery substrate was layered and powdery, with large and loose pores. White particles appear on the surface of the pottery figurines (Fig. 1). These glazed pottery figurines, which carry important historical and cultural information, are facing the dilemma of gradually disappearing.

In the article, the optical microscopy (OM), scanning electron microscopy equipped with energy dispersive X-ray spectrometry (SEM–EDS), energy X-ray fluorescence spectrometry (EDX), and micro-Raman spectroscopy are used for the first time to analyze the composition and structure of the surface corrosion materials of glazed pottery excavated from the tomb of Qibi Ming. For the first time, by extracting DNA and using ITS universal primers for amplification and sequencing, the microorganisms on the surface of glazed pottery are identified. For the first time, the cause of corrosion was analyzed and relevant models are established. This article provides new insights into the corrosion mechanism of glazed pottery, which is of great significance for protecting lead-glazed pottery.

## Materials and methods

### Sample preparation

In order to systematically study the corrosion of the glazed pottery from the tomb of Qibi Ming, six pieces of glazed pottery with different degrees of corrosion provided by the Xianyang Museum were used as the research objects of this article. The samples used were all small fragments of these glazed pottery pieces that fell


**Fig. 1** Photos of corroded glazed pottery

off due to corrosion. The sample numbers and photos are shown in Fig. 2.

### Cross-section sample preparation

The resin was used to fill half of the mold space and allowed to solidify at room temperature. The sample was placed on the cured resin surface, and the remaining space of the mold was filled with resin. After curing the upper layer of resin, the sample was extracted using a low-density cutter (Veiyee DTQ-5). The structure of the sample cross-section was examined with optical microscopy.

### Isolation and identification of microorganisms

The sterile cotton swab was dipped in sterile physiological saline to sample microorganism from the glazed pottery and then lined on potato dextrose agar (PDA) medium, which was incubated for 72 h at 28 ℃. The pure colonies were obtained using a sterile loop to scoop the single colonies to the sub-culture in a PDA medium. The identification of microorganism was acquired with the morphology Fungi and molecular biology techniques.

Genomic DNA was extracted from the isolates using a Tsingke Plant Mini Kit. The DNA was used as a template for ITS-PCR, with the primer pair ITS1 (5′- TCC GTAGGTGAACCTGCGG-3′) and ITS4 (5′- TCCTCC GCTTATTGATATGC-3′) [12]. PCRs were performed in 45 μL of Tsingke 1 × TSE101 Master Mix Kit. The cycling profile was as follows: initial denaturation at 98 ℃ for 2 min, followed by 38 cycles of denaturation at 98 ℃ for 10 s, annealing at 53 ℃ for 10 s, extension at 72 ℃ for 10 s, a final extension step at 72 ℃ for 5 min, and store at 4 ℃. The amplified PCR product was subjected to agarose gel electrophoresis (2 μl sample + 6ul bromophenol blue), and the identification gel map was obtained at 300 V for 12 min. The purified PCR products were sequenced using ITS1 and ITS4 primers at Tsingke. The generated sequences were matched to library sequences in the NCBI database. MEGA 11 software was used for multi sequence alignment.

### Methods

#### *Optical microscopy (OM)*

The morphology characteristics of glazed surfaces and cross-sections were observed by optical microscopy (Olympus BX53M) equipped with 10×, 20×, and 50× objective lens.

#### *Energy X-ray fluorescence spectrometry (EDX)*

The elemental characterization of glaze pottery was determined by EDX (Shimadzu EDX-7000). It was equipped with X-ray tube consisted of an Rh target and a silicon drift detector.

#### *Micro-Raman*

The phase components of the corrosive products were characterized using a laser micro-Raman spectroscopy (Renishaw, inVia Reflex). It was from 100 $cm^{-1}$ to 3500 $cm^{-1}$ using a grating with 400 lines/mm and a spot size of 2 μm, the excitation wavelengths were 532 and 785 nm. The objective lens magnification was 50× with an exposure time of 30 s. The accumulation period was 1 s using a laser power of 2mW. All spectral processing was performed using the instrument Wire software v. 3.4.

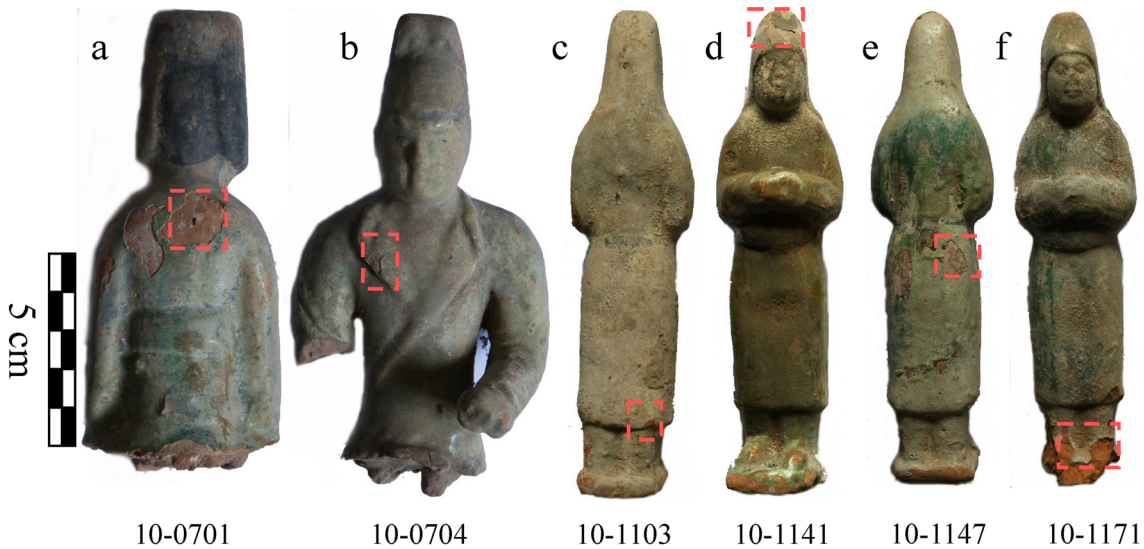


**Fig. 2** Images of the sampling position of samples, **a** 10–0701; **b** 10–0704; **c** 10–1103; **d** 10–1141; **e** 10–1147; **f** 10–1171

### *Scanning electron microscopy-energy dispersive X-ray spectrometer (SEM–EDS)*

The micromorphology of glaze surface and cross-sections were characterized using SEM (Hitachi SU8020) with a Horiba X-MAX80 EDS spectrometer. The tests were carried out in a vacuum environment with an operati voltage of 10 kV and element acquisition at a working distance of 15 mm for 1 min.

## Results

### Chemical composition of pristine pottery substrate and glaze layer

In order to comprehensively understand the chemical composition of the corroded area, the chemical composition of the substrate and glaze layer in the uncorroded area was first tested. Figure 3 shows the principal component analysis of pottery substrate and pristine glaze. In order to study the compositional characteristics of pottery substrate and original glaze, an OPLS-DA (Fig. 3a) model was established, which can effectively distinguish between pottery substrate and original glaze [13]. OPLS-DA analysis is a very powerful pattern recognition technique that can reduce the redundant information contained in n-dimensional patterns to two or three variables (principal components), and visualize the reduced data in parallel coordinates [14]. PC1 accounts for 71.5% of the contribution percentage, while PC2 accounts for 7% of the contribution percentage. PC1 positive values are influenced by PbO, and negative values by $Al_2O_3$ and $Fe_2O_3$. PC2 positive values are influenced by CuO, and negative values by $K_2O$ (Fig. 3b). The model validation is effective, there are significant differences in the composition between the pottery substrate and the original glaze.

Tables 1 and 2 show the EDX results for the chemical composition of the pottery substrate and glaze layer in an uncorroded. Based on the chemical composition, the content of $Fe_2O_3$ in the raw materials of all pottery substrate samples is above 6%, which is a common high iron fusible clay in northern China [15]. The raw materials for all samples of pottery substrate are high silicon (57.22–66.66%), low aluminum (13.67–17.38%), and low calcium (4.53–13.49%). These substances undergo chemical reactions at high temperatures, generating substances such as calcium silicate ($CaSiO_3$) and aluminum

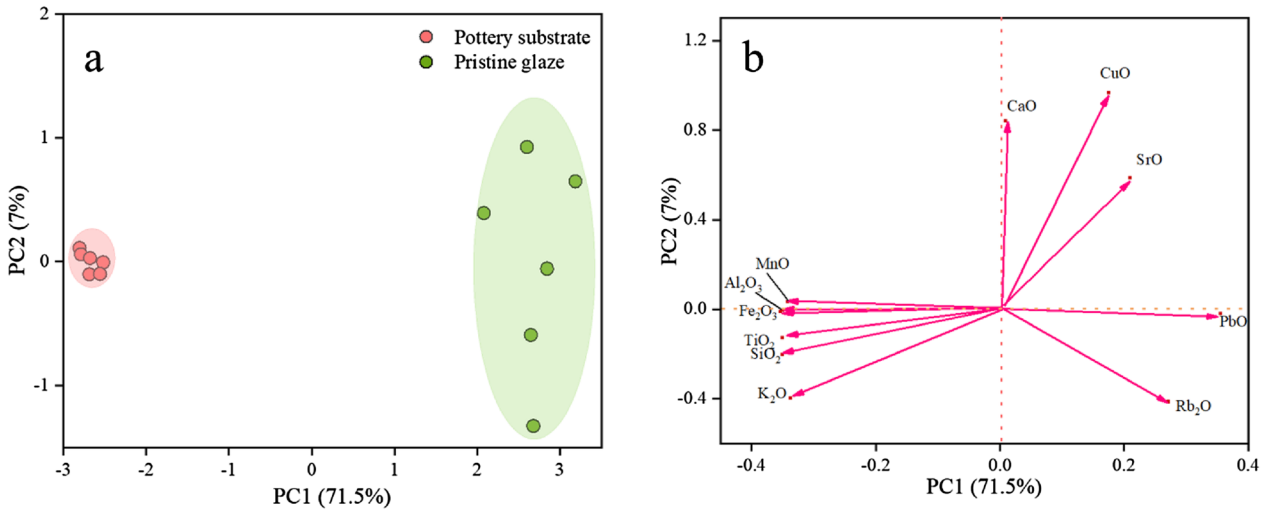


**Fig. 3** Principal component analysis of pottery substrate and pristine glaze, **a** OPLS-DA; **b** Load diagram

**Table 1** The main chemical composition of pottery substrate

| Sample (Wt%) | $SiO_2$ | $Al_2O_3$ | CaO | $Fe_2O_3$ | PbO | $K_2O$ | $TiO_2$ | SrO | MnO |
|---|---|---|---|---|---|---|---|---|---|
| 10–0701 | 57.22 | 14.11 | 13.49 | 7.08 | 2.51 | 3.62 | 1.04 | 0.11 | 0.14 |
| 10–0704 | 64.11 | 17.38 | 4.96 | 7.53 | 1.05 | 3.40 | 0.95 | 0.06 | 0.10 |
| 10–1103 | 62.23 | 13.67 | 8.95 | 6.39 | 3.71 | 3.64 | 0.96 | 0.14 | 0.12 |
| 10–1141 | 66.66 | 15.12 | 4.53 | 8.18 | 0.67 | 3.49 | 0.98 | 0.05 | 0.09 |
| 10–1147 | 65.39 | 16.38 | 5.63 | 7.27 | 0.71 | 3.29 | 0.94 | 0.06 | 0.10 |
| 10–1171 | 66.34 | 16.34 | 4.84 | 7.04 | 0.62 | 3.43 | 0.91 | 0.05 | 0.09 |

**Table 2** The main chemical composition of pristine glaze

| Sample (Wt%) | PbO | $SiO_2$ | CaO | $Fe_2O_3$ | CuO | SrO | $K_2O$ | $TiO_2$ | $Rb_2O$ |
|---|---|---|---|---|---|---|---|---|---|
| 10–0701 | 85.48 | 9.44 | 2.42 | 0.53 | 1.26 | 0.50 | – | – | 0.02 |
| 10–0704 | 69.44 | 10.54 | 13.56 | 1.41 | 2.07 | 0.81 | 1.37 | 0.32 | 0.03 |
| 10–1103 | 67.27 | 24.41 | 5.40 | 0.90 | 0.16 | – | 1.43 | 0.27 | 0.12 |
| 10–1141 | 67.04 | 11.10 | 10.40 | 0.66 | 9.81 | – | – | – | 0.04 |
| 10–1147 | 75.27 | 10.67 | 8.17 | 0.73 | 1.32 | 0.91 | 0.27 | 0.14 | 0.13 |
| 10–1171 | 75.26 | 14.57 | 5.22 | 0.79 | 1.55 | 0.36 | 1.68 | 0.15 | 0.07 |

silicate ($Al_2SiO_5$), thus forming hard pottery substrate [16]. The content of $K_2O$ is all above 3%, and as a flux, it can reduce the firing temperature of the pottery substrate [17, 18]. The pottery substrate contain trace amounts of PbO, which is due to the volatilization of a small amount of PbO into the pottery substrate during high-temperature firing. The high content of PbO in the original glaze layer indicates that the glaze layer uses Pb as a flux [4]. The polarization effect of Pb reduces the fracture temperature of Si–O bonds, thereby lowering the melting temperature of the glaze [13]. The color of lead-glaze pottery mainly depends on the composition and content of colorant agent, as well as firing atmosphere. When the colorant is Fe, it appears red, yellow, brown, and brown in the oxidizing atmosphere, and blue and black in the reducing atmosphere. If the colorant element is Cu, it appears green in the oxidizing atmosphere and red in the reducing atmosphere [19–21]. In this article, the glaze color is mainly light yellowish green with Fe as the colorant agent and green with Cu as the colorant agent, indicating that the glaze pottery figurines were fired in an oxidizing atmosphere. After removing PbO and colorants from the glaze layer, the components were normalized. The content of $SiO_2$ and CaO were higher than that of the pottery substrate, indicating that the glazed pottery belongs to PbO–CaO–$SiO_2$ mixed glaze.

### Optical microscopy images of corroded areas

The Optical microscopy images of the corroded area of the glaze layer are shown in Fig. 4. The glaze layer on the surface of the samples has varying degrees of corrosion. There is a clear scratch on the surface of the glaze layer of 10–0701 sample (Fig. 4a), and white corrosive substances are produced near the scratch. The corroded area of 10–0704 sample (Fig. 4b), the bond between the glaze layer and the pottery substrate is not tight enough, and some areas of the glaze surface are severely peeled off, even exposing the pottery substrate. The surface of the glaze layer is also accompanied by a silver white glossy covering layer, which is called "silver glaze" [22, 23]. The 10–1103 (Fig. 4c) sample shows turtle cracks in the glaze layer and white corrosion, with some pottery substrates exposed on the surface. The green glaze layer of 10–1141 (Fig. 4d) sample is relatively intact, and the surface is

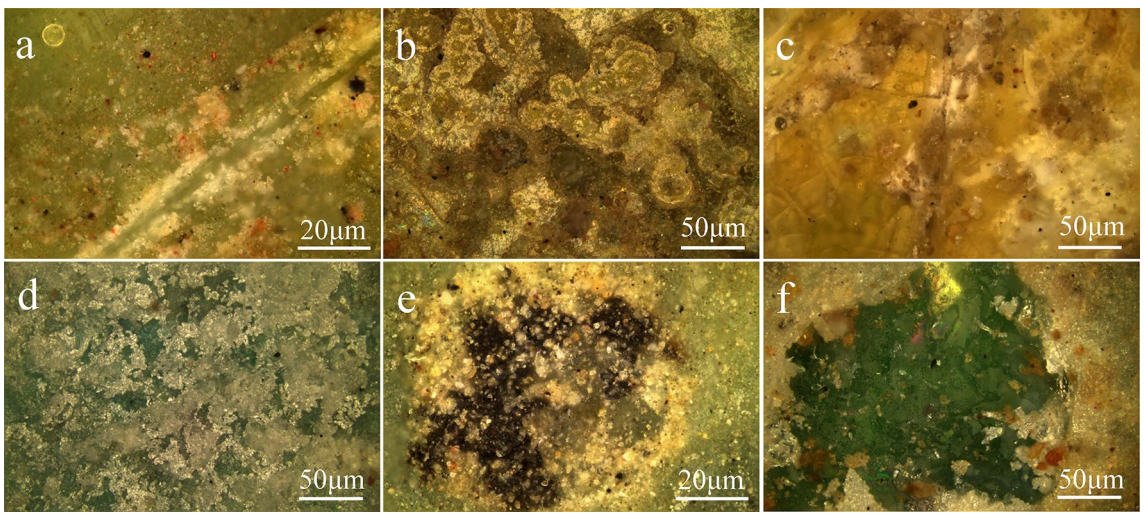


**Fig. 4** Optical microscopy images of samples, **a** 10–0701; **b** 10–0704; **c** 10–1103; **d** 10–1141; **e** 10–1147; **f** 10–1171

covered with loose white corrosive substances. The black corrosion pit appears on the surface of the green glaze in 10–1147 sample (Fig. 4e). The green glaze layer of 10–1171 sample (Fig. 4f) is basically covered by dense white corrosive substances.

### The composition of the corroded areas

The main chemical composition of the corroded areas of the glaze layer are shown in Table 3. The content of PbO in all samples has decreased, indicating the possible generation of lead related corrosive substances. The content of CaO in the 10–1103 sample increased significantly, possibly due to the presence of calcium related compounds near the glazed pottery. In addition, Cl element is found in the 10–1141 and 10–1171 samples. According to Table 2, there is no Cl element in the pristine glaze layer, indicating that the Cl element comes from the burial environment before excavation. Figure 5 shows the SEM and EDS of soluble salts on the corroded surfaces of the 10–1141 and 10–1171 samples. After testing, it was found that the main component of soluble salts is NaCl, indicating that the soil used for burying glazed pottery should contain NaCl.

### Microstructure and composition of the corrosion layer

The microstructure and Raman spectroscopy of the corroded area are shown in Figs. 6 and 7. The scratch on 10–0701 sample (Fig. 6a) is shallow and don't expose

**Table 3** The main chemical composition of corroded glaze layer

| Sample (Wt%) | PbO | $SiO_2$ | CaO | $Fe_2O_3$ | CuO | SrO | $K_2O$ | $TiO_2$ | $Rb_2O$ | Cl |
|---|---|---|---|---|---|---|---|---|---|---|
| 10–0701 | 70.90 | 20.88 | 5.48 | 0.85 | – | 0.36 | 0.96 | 0.19 | 0.03 | – |
| 10–0704 | 62.69 | 20.67 | 9.63 | 0.98 | 1.76 | 0.79 | 0.88 | 0.23 | – | – |
| 10–1103 | 42.29 | 11.48 | 42.51 | 1.80 | – | 0.32 | 1.05 | 0.17 | 0.03 | – |
| 10–1141 | 56.99 | 16.22 | 5.09 | 0.61 | 5.71 | – | 0.18 | – | 0.11 | 14.80 |
| 10–1147 | 70.10 | 20.48 | 4.47 | 0.71 | – | 0.87 | 0.53 | – | 0.03 | – |
| 10–1171 | 59.78 | 13.35 | 3.69 | 0.68 | 0.82 | 0.20 | 2.49 | 0.18 | 0.05 | 18.76 |

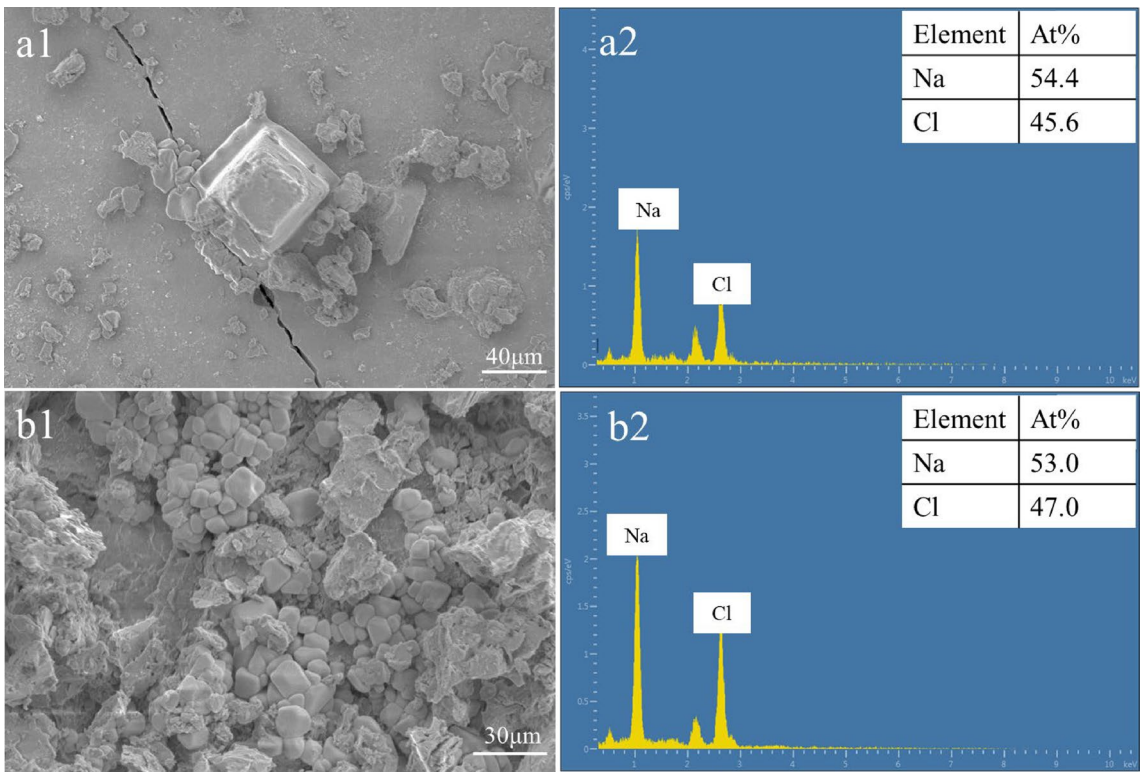


**Fig. 5** SEM (**a1** 10–1141; **b1** 10–1171) and EDS (**a2** 10–1141; **b2** 10–1171) of crystalline salts in the sample

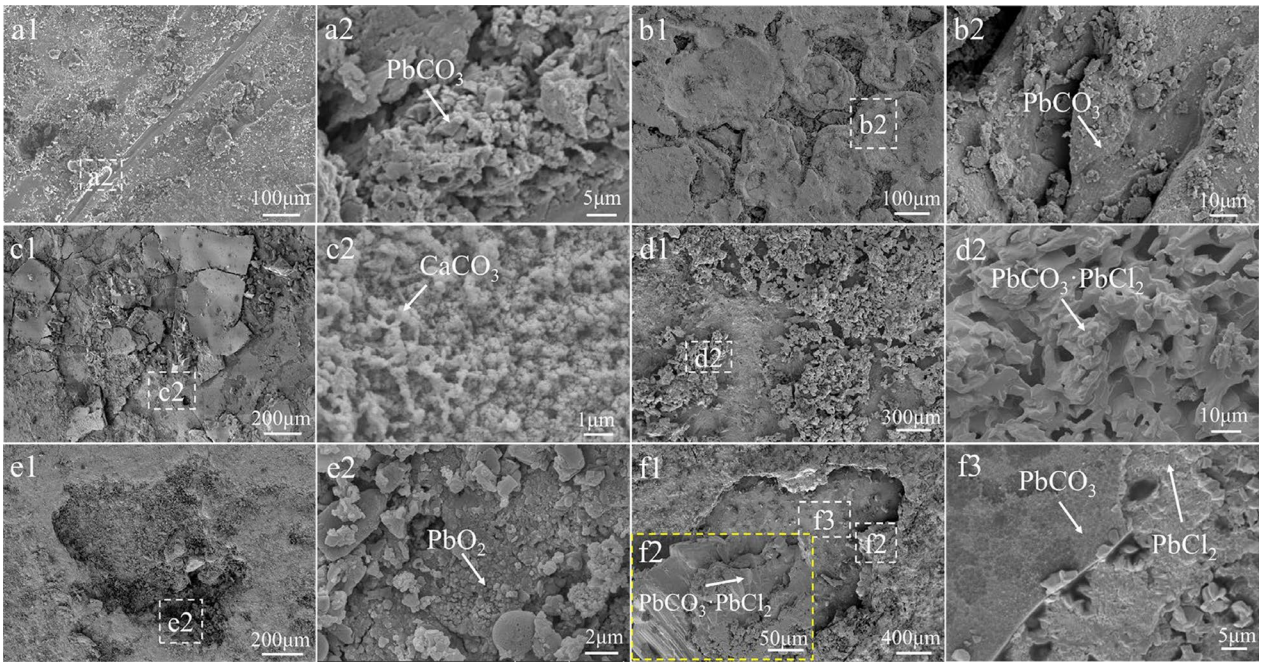


**Fig. 6** SEM of corrosive substances of samples, **a1**, **a2** 10–0701; **b1**, **b2** 10–0704; **c1**, **c2** 10–1103; **d1**, **d2** 10–1141; **e1**, **e2** 10–1147; **f1**, **f2, f3** 10–1171

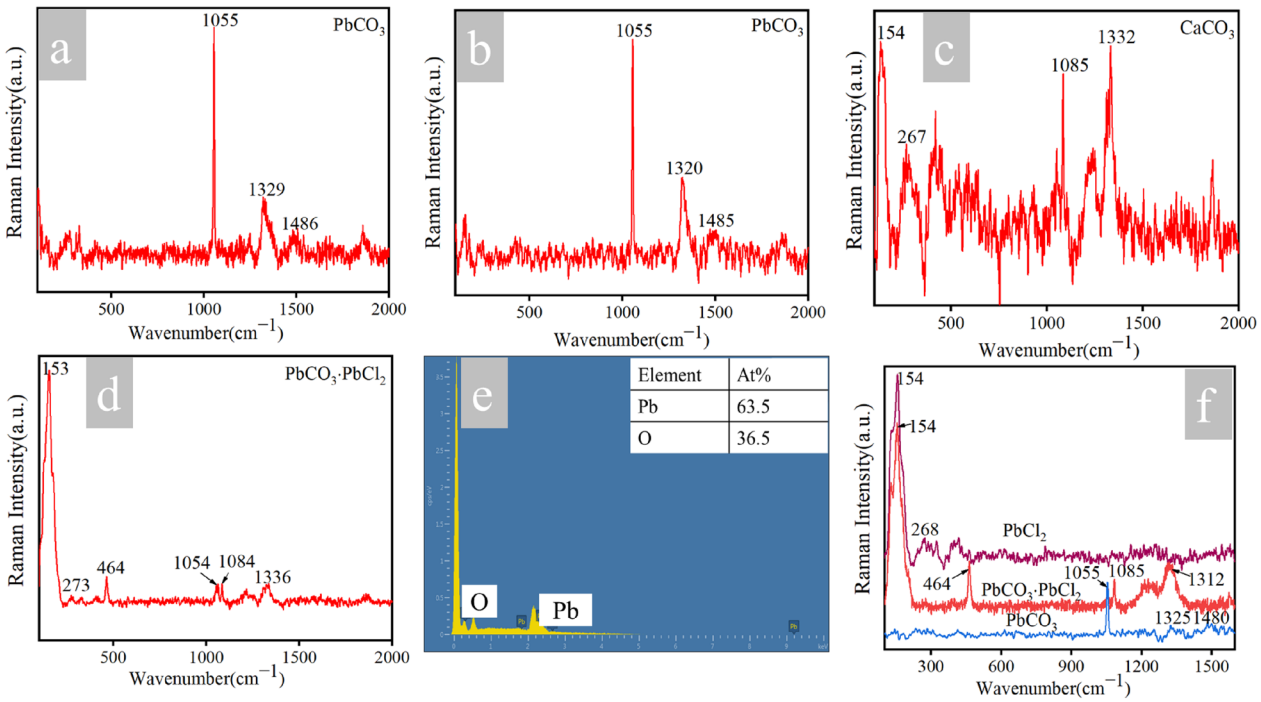


**Fig. 7** EDS and Raman spectroscopy of corrosive substances of samples, **a** 10–0701; **b** 10–0704; **c** 10–1103; **d** 10–1141; **e** 10–1147; **f** 10–1171

the pottery substrate. The white corrosive substance near the scratch is granular. Raman testing is performed on the white corrosive substance (Fig. 7a), the main Raman peaks are recorded at 1055 $cm^{-1}$, 1329 $cm^{-1}$, and 1486 $cm^{-1}$, which are the characteristic peak of cerussite ($PbCO_3$) [24–26]. The corrosion surface of the 10–0704 (Fig. 6b) sample is a relatively loose layered structure, with Raman characteristic peaks of 1055 $cm^{-1}$,

1329 $cm^{-1}$, and 1485 $cm^{-1}$ (Fig. 7b), which are consistent with the characteristic peaks of sample 10–0701 and also belong to $PbCO_3$ [22, 23]. A large number of turtle cracks exist on the surface of the 10–1103 sample (Fig. 6c), the surface of the glaze layer is loose, and the white corrosive substance is in the form of aggregated small particles. The main Raman peaks are observed at 154 $cm^{-1}$, 267 $cm^{-1}$, 1085 $cm^{-1}$, and 1332 $cm^{-1}$. This is the characteristic peak of calcite ($CaCO_3$) (Fig. 7c) [27–29]. The white corrosive substance on the surface of the 10–1141 (Fig. 6d) sample is relatively loose, with pores, and the surface is relatively smooth and irregular. The main Raman peaks are recorded at 153 $cm^{-1}$, 273 $cm^{-1}$, 464 $cm^{-1}$, 1054 $cm^{-1}$, 1084 $cm^{-1}$, and 1336 $cm^{-1}$, this is the characteristic peak of phosgenite ($PbCO_3 \cdot PbCl_2$) (Fig. 7d) [30]. The surface of the 10–1147 sample is a black corrosion pit (Fig. 6e). EDS testing was conducted on the black corrosion part, and it was found that only two elements, Pb and O (Fig. 7e), were present, indicating that the black corrosion substance should be $PbO_2$ [31]. The corrosion composition on the surface of the 10–1171 sample is relatively complex (Fig. 6f). In addition to $PbCO_3$ and $PbCO_3 \cdot PbCl_2$ mentioned in the previous corrosion, the presence of lead chloride ($PbCl_2$) was also detected (Fig. 7f) [32, 33].

### Cross-section corrosion analysis

The cross-sections of 10–1103 and 10–1171 samples are significantly corroded, and the corrosion products are tested. Figures 8 and 9 show the OM, SEM and EDS element maps of the cross-sections of 10–1103 and 10–1171 samples, respectively. V-shaped cracks are observed on the profiles of the 10–1103 and 10–1171 samples, which are typical structures of lead-glaze crack corrosion [4]. The corrosion layer that first forms in the crack is located in the center of the crack, while on the glaze, it is at the top of the entire corrosion layer. The bottom layer of the corrosion layer extends closely to the glaze and extends all the way to the V-shaped inner wall. The "V"—shaped structure is formed after long-term corrosion of cracks, and finally forms a layer close to the glaze layer and the "V"—shaped inner wall·

Compared to the composition of the pristine glaze, the Si element in the red line area (Fig. 8c) is significantly higher than Pb, indicating that it should be a Si-rich layer. The lead-glaze pottery was eroded by water in the buried environment, and some preferred components in the glass phase (mainly alkali metals, alkali earth metals, lead oxides, etc.) were transferred into the environmental medium, $H^+$ undergoes ion exchange with dissolved ions such as $K^+$, $Pb^{2+}$, $Cu^{2+}$ in the glaze. $Si(OH)_4$ is a polar molecule that adsorbs surrounding water molecules to form alkali deficient silicon gel $Si(OH)_4 \cdot n(H_2O)$, also known as Si-rich layer [1, 4]. Through EDS element maps, it was found that the white corrosive area of 10–1171 cross-section is mainly composition of Pb and Cl, with relatively low content of O and Si elements, and no content of C element. Combined the Raman results in Fig. 7f, it is indicated that $PbCl_2$ is present of 10–1171 sample, and the white corrosion material here should be $PbCl_2$.

### Isolation and identification of microorganisms on corroded surfaces

Microbial hyphae and spores appeared on the surface of 10–0701 sample, and microbial corrosion pits appeared (Fig. 10). Two microbial colonies, numbered a and b, are isolated and purified from the surface of lead-glazed

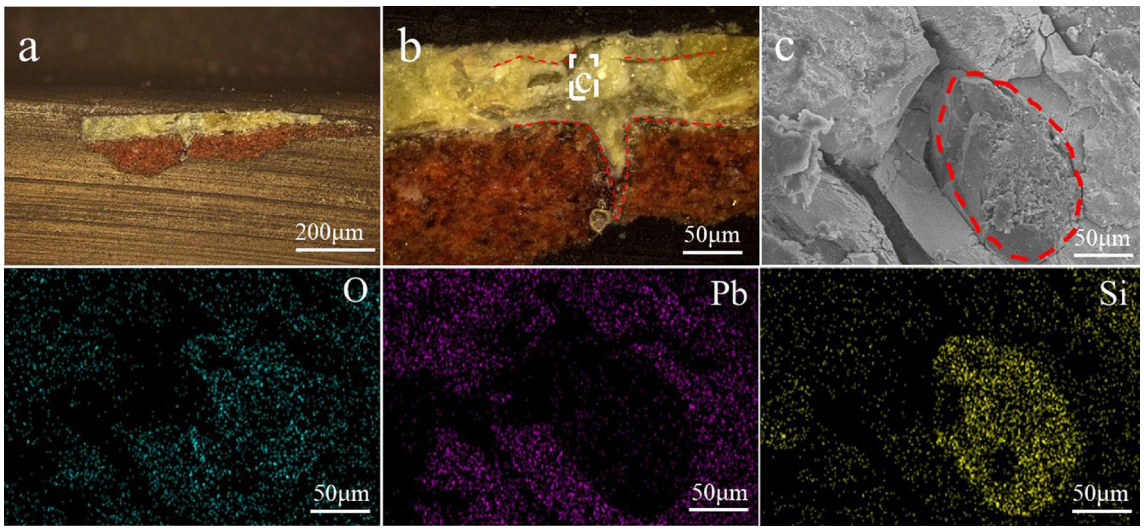


**Fig. 8** OM (**a**, **b**), SEM (**c**) and EDS element maps of the cross-section of 10–1103 sample

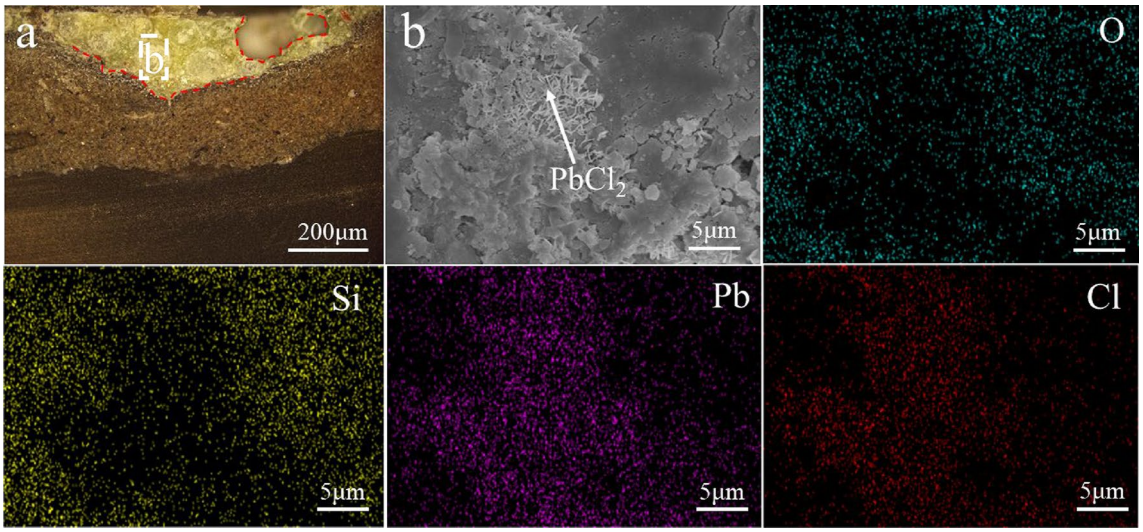


**Fig. 9** OM (**a**), SEM (**b**) and EDS element maps of the cross-section of 10–1171 sample

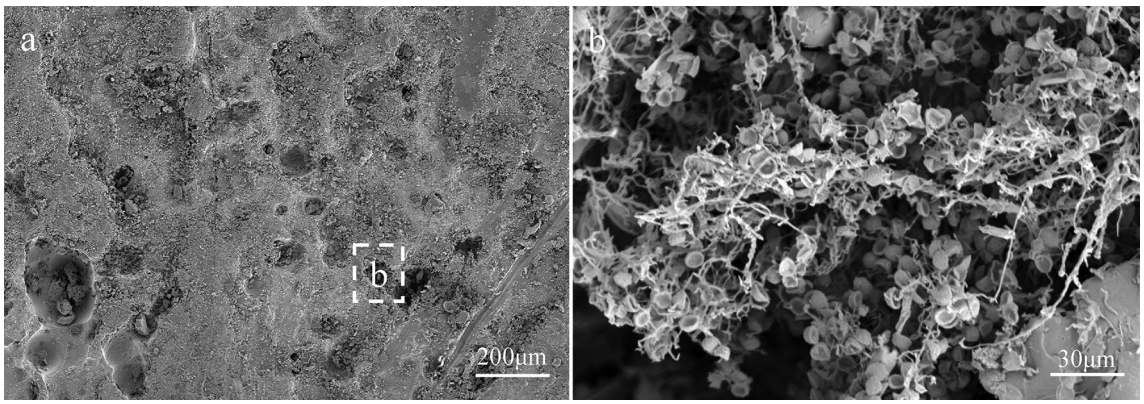


**Fig. 10** **a** Microbial corrosion pits; **b** growth spores on the surface of 10–0701

pottery. Cultivate each strain according to the microbial morphology cultivation method. The colony morphology and microscopic morphology characteristics of each strain on PDA medium are shown in Fig. 11. Based on the sequencing results, the obtained gene sequence will be homologously compared with the gene sequences included in the NCBI nucleic acid sequence database, and the sequence with the highest score in the database will be selected as the reference object. Based on the phylogenetic tree analysis results (Fig. 12), combined with the morphological characteristics and homology comparison results of different strains, the phylogenetic relationship between the two strains was determined. Finally, it was determined that the two microorganisms were *Aspergillus niger* and *Aspergillus sclerotiorum*. Both *Aspergillus niger* and *Aspergillus sclerotiorum* belong to the fungal kingdom. *Aspergillus niger* is widely distributed in soil and plants around the world, with a fast growth rate. On PDA medium, the colonies are flat and olive black, and the surface of the colonies is smooth and even. The microscopic morphology of the spores is spherical or radial, resembling chrysanthemums, with a brown black color. *Aspergillus sclerotiorum* widely grows in soil and medicinal materials, with a flocculent texture mainly concentrated in the center of the colony and faint yellow color. The microscopic morphology is spherical or nearly spherical, with smaller conidia.

## Discussion

In this section, the principle of corrosion products were analyzed, and the cultural relics were modeled based on the corrosion mechanism, clearly expressing the process of cultural relics being corroded (Fig. 13).

The glaze is a thin glass layer covering the pottery substrate. Glaze is made from mineral materials in a certain ratio and applied to the surface of the pottery substrate. It

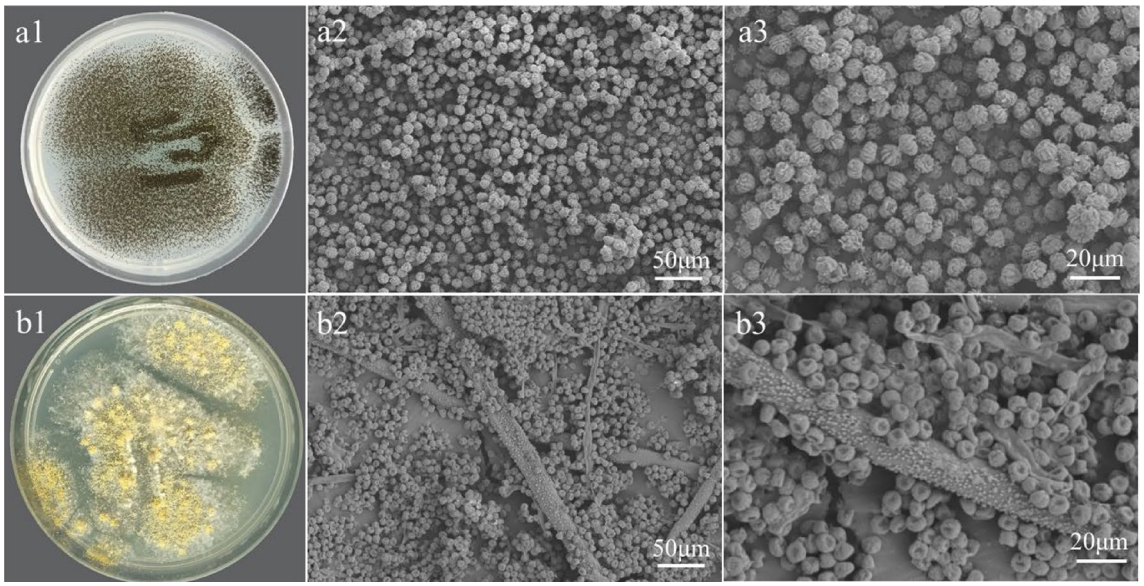


**Fig. 11** Morphology (**a1**, **b1**) and Microscopic morphology diagram (**a2**, **a3**, **b2**, **b3**) of microorganism colony

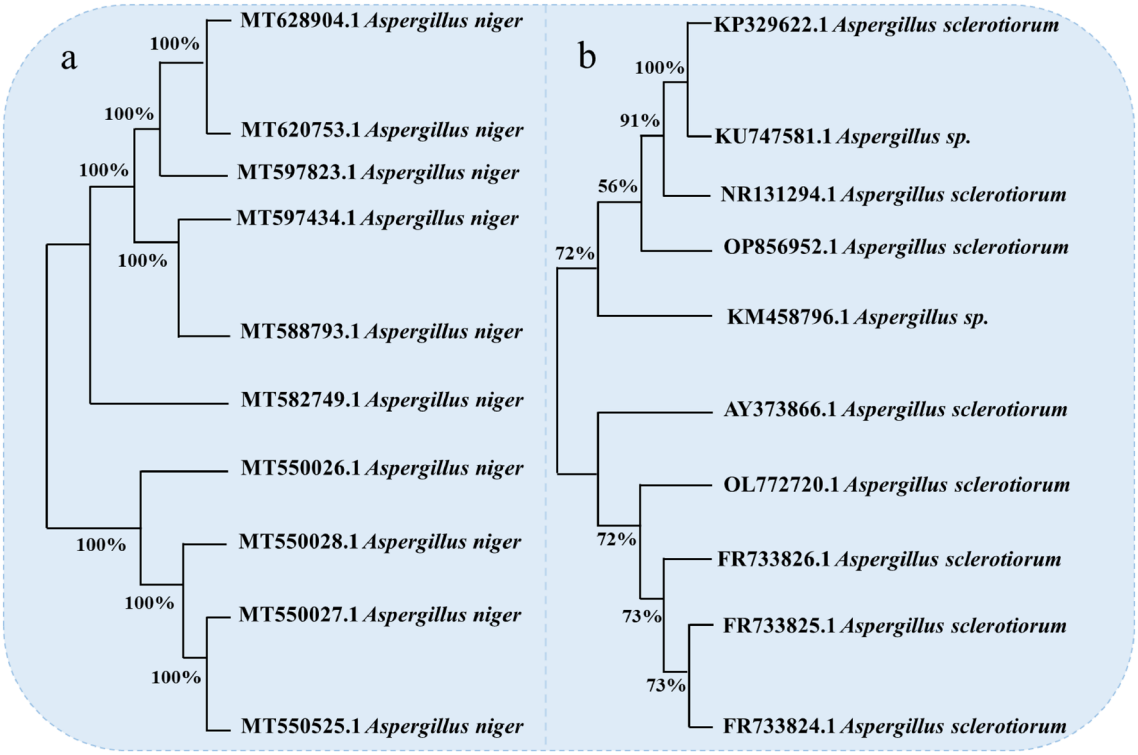


**Fig. 12** Phylogenetic tree of ITS sequence of microorganisms, **a** *Aspergillus niger*; **b** *Aspergillus sclerotiorum*

is then calcined at a certain temperature. Due to the high refractive index of the glass layer of lead glazed pottery, its surface is clearer and more transparent than other glazed pottery, shining brightly. The glaze is considered to be chemically stable and able to resist most environmental erosion except strong acids and alkalis. But the surface of the glazed pottery (10–0704) excavated from the Qibi Ming tomb lost its pristine luster, and a layer of

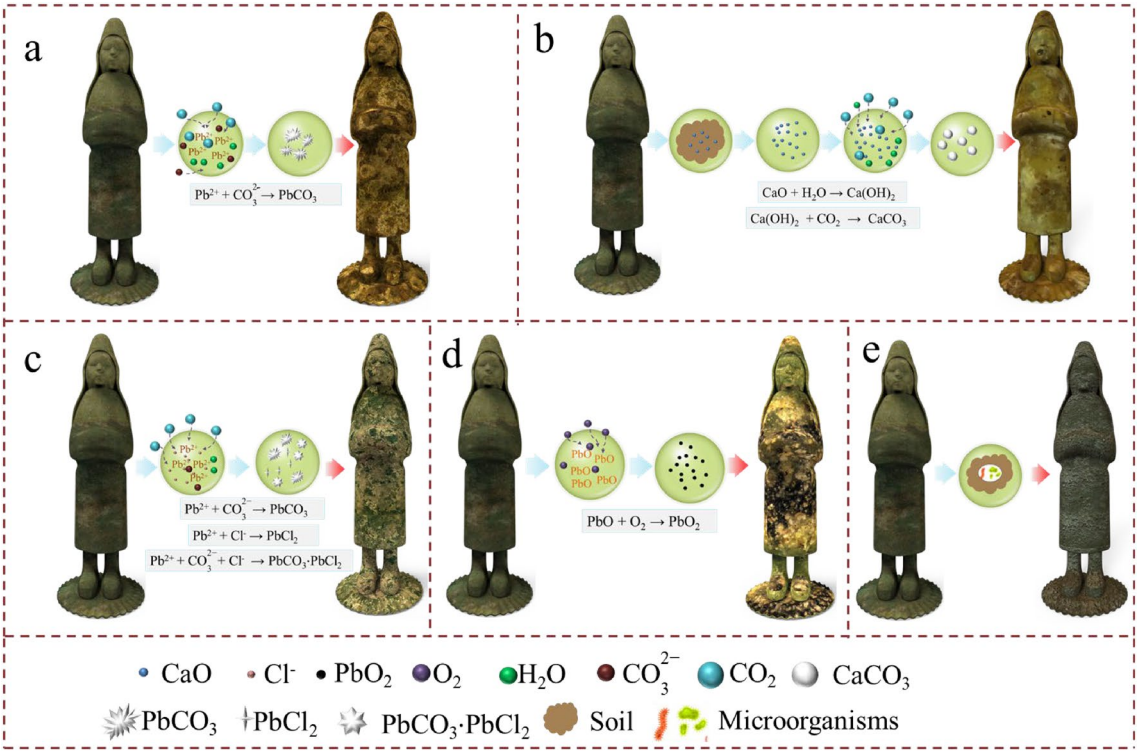


**Fig. 13** Schematic diagram of glazed pottery corrosion, **a** $PbCO_3$; **b** $CaCO_3$; **c** $PbCl_2$ and $PbCO_3 \cdot PbCl_2$; **d** $PbO_2$; **e** microorganisms

silver white metallic luster appeared on the glaze, known as "silver glaze" [34]. Silver glaze is an amorphous substance with a layered structure. The formation of silver glaze is mainly due to the dissolution of $Pb^{2+}$ from the surface of low-temperature lead green glaze, which reacts with carbonate ions in the soil or water and carbon dioxide in the air ($Pb^{2+} + CO_3^{2-} \rightarrow PbCO_3$). A layer of sediment (mainly composed of lead ore $PbCO_3$) is formed in the contact layer [33, 35]. Due to the insufficient bonding between the sediment and the glaze layer, there are gaps, and air can still penetrate through them to corrode the glaze layer. Over time, this process is repeated, resulting in an increasing number of sediment layers and a thickening of the sediment layer. This corrosion mechanism can be attributed to dissolution–precipitation. At this point, the sediment layer exhibits a silver white luster under the interference of light (Fig. 13a). $PbCO_3$ was also detected on the surface of 10–0701 sample, due to the presence of scratches on its surface. More $Pb^{2+}$ dissolved near the scratches came into contact with carbonate ions or water and carbon dioxide in the air, preferentially generating $PbCO_3$, resulting in obvious white corrosion on its surface.

$CaCO_3$ is detected in the corroded area of 10–1103 sample, and the content of CaO is significantly higher than that in the uncorroded area. The tomb of Qibi Ming is located in the northwest of Xianyang, China. The soil here is weakly alkaline, with a pH of 7.5–8.5 [36–38]. This indicates that the soil in which glazed pottery is buried should contain alkaline metal oxides, such as CaO and MgO. During the thousands of years of burial, CaO in the soil deposited onto the surface of glazed pottery. After the excavated glazed pottery, the surface CaO reacted with $H_2O$ and $CO_2$ in the air, generating $CaCO_3$ ($CaO + H_2O \rightarrow Ca(OH)_2$, $Ca(OH)_2 + CO_2 \rightarrow CaCO_3$) (Fig. 13b) [39].

A large amount of $Cl^-$ is detected in the corroded areas of 10–1141 and 10–1171 samples, which are derived from NaCl, indicating the presence of a large amount of soluble salt NaCl in the soil of buried glazed pottery. The $Pb^{2+}$ on the surface of glazed pottery and the $CO_3^{2-}$ generate $PbCO_3$, and some $Pb^{2+}$ undergoes reaction with $Cl^-$ in soluble salts to generate $PbCl_2$ ($Pb^{2+} + Cl^- \rightarrow PbCl_2$) [33]. $Pb^{2+}$, $Cl^-$, and $CO_3^{2-}$ undergo long-term action to generate $PbCO_3 \cdot PbCl_2$ ($Pb^{2+} + Cl^- + CO_3^{2-} \rightarrow PbCO_3 \cdot PbCl_2$), causing severe corrosion on the surface of glazed pottery (Fig. 13c). On the surface of 10–1141 sample, there is only $PbCO_3 \cdot PbCl_2$, and the morphology of the corrosion products is basically consistent (Fig. 6d), indicating that $Pb^{2+}$, $CO_3^{2-}$ and $Cl^-$ fully react. The corrosion on the surface of 10–1171 sample is relatively complex, with $PbCO_3 \cdot PbCl_2$ covering the surface of the glaze layer, and

$PbCl_2$ and $PbCO_3$ present on the surface of the uncovered glaze layer (Fig. 6f), indicating that the combination reaction of the two is the main reason for the appearance of a large amount of white corrosion on the surface of the terracotta figurine. Due to $CO_3^{2-}$ was present only on the surface of the pottery figurine, the corrosion product in the cross-section of 10–1171 sample was only $PbCl_2$.

The black corrosion pit appears on the surface of the green glaze in 10–1147 sample. After excavation, the surface of the glazed pottery is exposed to the air for a long time, fully in contact with the $O_2$ in the air, causing oxidation reaction between PbO and $O_2$, generating black corrosive substance $PbO_2$ ($PbO + O_2 \rightarrow PbO_2$) (Fig. 13d) [31].

During the burial process of glazed pottery, due to the presence of microorganisms in the soil, these microorganisms can cause biological corrosion on the surface of glazed pottery. Through collection, separation, and identification, it was found that the microorganisms on the surface of glazed pottery mainly refer to two types of fungi, namely *Aspergillus niger* and *Aspergillus sclerotiorum*. These two varieties of fungi exude numerous pigments throughout their life cycle, resulting in the formation of variously colored fungal patches that obscure the original aesthetic of glazed pottery. Additionally, these fungi generate organic acids as part of their metabolic processes, which disrupt the integrity of the PbO-$CaO$-$SiO_2$ network within the glass phase, causing the breakdown of the glass structure and the rapid release of metal oxide ions such as Ca, K, and Fe. This phenomenon leads to the development of corrosion pits on the surface of the glazed pottery, ultimately compromising its resistance to corrosion. (Fig. 13e) [40–42].

## Conclusion

Based on the OM, EDX, SEM–EDS, and micro-Raman spectroscopy, it was determined that the lead-glazed pottery excavated from the tomb of Qibi Ming consists of low-temperature PbO-$CaO$-$SiO_2$ glaze, with Pb as the primary flux, and Cu, Fe as the main colorants. The corrosion observed on the lead-glazed pottery figurines includes both chemical and microbial corrosion. The main corrosion products include $PbCO_3$, $CaCO_3$, $PbCl_2$, $PbCO_3$·$PbCl_2$, and $PbO_2$. In addition, "V"-shaped cracks are found in the cross-section of 10–1103 and 10–1171 samples, with Si-rich area found in the cross-section of 10–1103 sample. By extracting DNA and using ITS universal primers for amplification and sequencing, the microorganisms on the surface of glazed pottery are identified. It was found that the mainly contains two types of microorganisms, namely *Aspergillus niger* and *Aspergillus sclerotiorum.*

The different corrosion models are built by identifying the corrosion products and types. Chemical corrosion is mainly caused by dissolution precipitation, chemical reactions, and oxidation reactions. These reactions lead to the formation of "silver glaze", white corrosive substances, and black corrosion pits on the surface of the pottery figurines. The organic acids and fungus spots produced by microorganisms during their growth process are the main causes of biological corrosion. This study provides vital reference value for excavated and protection research of lead-glazed pottery.

**Acknowledgements**
The authors are grateful to the Xianyang Museum for the support with the samples for this research.

**Author contributions**
YL (Yanli Li): Writing- original draft, Investigation, Funding acquisition. PL: Writing-review. YL (Yujia Luo): Writing-review, Funding acquisition. MG: Data curation. HX: Conceptualization, Funding acquisition. YL (Yuhu Li): Supervision.

**Funding**
This research was supported by the Young Scientist Initiative Project of the School of Materials Science and Engineering at the Shaanxi Normal University (2023YSIP-MSE-SNNU003), the Fundamental Innovation Project in the School of Materials Science and Engineering (SNNU), the Fundamental Research Funds for the Central Universities (GK 202205025), the Fundamental Research Funds for the Central Universities (GK 202304013), and the Shaanxi Key Research and Development Program of China (2024GX-YBXM-560).

**Availability of data and materials**
The raw data required to reproduce these findings cannot be shared at this time as the data also forms part of an ongoing study.

## Declarations

**Competing interests**
The authors declare that they have no competing interests.

Received: 15 April 2024 Accepted: 22 June 2024
Published online: 03 July 2024

**References**

1. Zhou B, Ma Q, Li Z, Zhang Z, Li N. Corrosion of glaze in the marine environment: study on the green-glazed pottery from the Southern Song "Nanhai I" shipwreck (1127–1279 A.D). Herit Sci. 2023;11:134–52. https://doi.org/10.1186/s40494-023-00965-w.
2. Wang Y, Ma H, Chen K, Huang X, Cui J, Sun Z, et al. Identification of PbO (BaO) faience from an early and middle Warring States period cemetery at Zhaitouhe, northern Shaanxi. China Archaeometry. 2018;61:43–54. https://doi.org/10.1111/arcm.12401.
3. Luo D, Zheng J. New archaeological progress in lead glazed pottery kiln sites from the Han Dynasty to the Southern and Northern Dynasties since the 21st century. Cult Relics World. 2022;09:112–8.
4. Jiang F, Li Z, Wei S, Song Y, Ma Q. Research on the corrosion of lead-glazed pottery from Cizao kiln of the Song Dynasty in Jinjiang, Fujian Province. Sci Conserv Archaeol. 2021;33:71–9. https://doi.org/10.16334/j.cnki.cn31-1652/k.20201001902.
5. Geng Q. Analysis on glass attributes of glaze. Jiangsu Ceram. 2002;35:10–2. https://doi.org/10.16860/j.cnki.32-1251/tq.2002.03.004.
6. Zhang K, Wu C, Zhao J, Yu W, Zhao M. The corrosion mechanism of lead-glazed pottery in Han dynasty. Npj Mat Degrada. 2024;8:1–12. https://doi.org/10.1038/s41529-024-00428-y.
7. Li Z, Ma Y, Ma Q, Chen J, Song Y. New perspective on Jun glaze corrosion: study on the corrosion of light greenish blue and reddish purple glazes

from Juntai Kiln, Yuzhou, Henan. China Herit Sci. 2020;8:1–11. https://doi.org/10.1186/s40494-019-0346-y.
8. Bette S, Eggert G, Fischer A, Stelzner J, Dinnebier RE. Characterization of a new efflorescence salt on calcareous historic objects stored in wood cabinets: $Ca_2(CH_3COO)(HCOO)(NO_3)_2{\cdot}4H_2O$. Corro Sci. 2018;132:68–78. https://doi.org/10.1016/j.corsci.2017.12.020.
9. Jie F, Ma X. Excavation of Qibi Ming's Tomb. Washington: Relics and Museology; 1998. p. 11–5.
10. Wang Y, Liu X. The rare Tang Tri-colored glazed pottery unearthed from the tomb of Qibi Ming. Collections. 2011;224:31–4.
11. Li Y, Guo H, Xiao K, Liu P, Chao X, Fu P, et al. A study of pigment, adhesive, and firing temperature in pottery figurines excavated from the Tomb of Qibi Ming. Chin Mol. 2023;28:1–13. https://doi.org/10.3390/molecules28237739.
12. Liu N, Chu D, Chen X, Fu P, Xing H, Chao X, et al. A spray-on microemulsion with mold-proof effect on paper. Coatings. 2023;13:1–12. https://doi.org/10.3390/coatings13040745.
13. Alonso-Olazabal A, Ortega LA, Zuluaga MC, Alonso-Fernández C, Jimenez-Echevarría J, Sarmiento A. Glaze characterization of the glazed pottery from the medieval workshop of Vega (Burgos, Spain). J Raman Spectrosc. 2022;53:1204–13. https://doi.org/10.1002/jrs.6328.
14. Fu Y, Huang Y, Zong S, Jiang J, Wang A, Xiao B, et al. Identification and classification of six kinds of proteinaceous binding media by THM-Py-GC/MS. Sci Conserv Archaeol. 2022;34:22–31.
15. Du X, Cui J. Scientific analysis of Han Dynasty Lead-barium polychrome glazed pottery excavated from Yan'an, Shaanxi province. Collect Stud Archaeol. 2022;02:247–59.
16. Legodi MA, de Waal D. Raman spectroscopic study of ancient South African domestic clay pottery. Spectrochim Acta A. 2007;66:135–42. https://doi.org/10.1016/j.saa.2006.02.059.
17. Xiong Y. Research on chemical composition of green glaze of ceramics in different periods in ancient China. Chin Ceram. 2014;50:87–92. https://doi.org/10.16521/j.cnki.issn.1001-9642.2014.08.030.
18. Tseng YK, Xu BY. An analysis of the gem-blue glaze of Ye Wang's Koji Pottery. Archaeometry. 2012;54:643–63. https://doi.org/10.1111/j.1475-4754.2011.00646.x.
19. Liu G, Jia Y, Tang H. Analysis and study of glazed pottery figurines excavated from Sima Jinlong Tomb of Northern Wei Dynasty. Journal of Chinese Antiquity. 2023;3:113–8.
20. Yu Y, Wang X. Detection and analysis of lead glazed pottery unearthed from the tomb of the Waring States Period in Linzi Shangdong. Human Cultural Heritage Perservation. 2016: p. 50–53.
21. Wu B, Zhao W, Ren X, Liu X, Li B, Feng S, et al. Firing process and colouring mechanism of black glaze and brown glaze porcelains from the Yuan and Ming dynasties from the Qingliang Temple kiln in Baofeng, Henan. China Ceram Int. 2021;47:32817–27. https://doi.org/10.1016/j.ceramint.2021.08.178.
22. He Q, Lv S, Pei Y, Li Y, Zhao R. Formation and analysis of corrosion products on green yellow glazed pottery from the Caocun kiln. Sci Conserv Archaeol. 2014;26:16–21. https://doi.org/10.16334/j.cnki.cn31-1652/k.2014.02.006.
23. Zhang F, Zhang Z. Low-temperature coloured glzaes of succesive dynaties in ancient China. J Chin Ceram Soc. 1980;8:9–19.
24. Lee NR, Yun JH, Kim SJ. Raman spectroscopy of yellow organic pigments of large Korean Buddhist paintings from the late Joseon dynasty (17th–19th centuries). J Raman Spectrosc. 2023;54:836–46. https://doi.org/10.1002/jrs.6565.
25. Yin X, Huang TJ, Gong H. Chemical evolution of lead in ancient artifacts—a case study of early Chinese lead-silicate glaze. J Eur Ceram Soci. 2020;40:2222–8. https://doi.org/10.1016/j.jeurceramsoc.2020.01.002.
26. Marutoiu C, Bratu I, Nemes OF, Dit I-I, Comes R, Tanaselia C, et al. Instrumental analysis of materials and topology of the Imperial Gates belonging to the Apahida wooden church. Cluj County Vib Spectrosc. 2017;89:131–6. https://doi.org/10.1016/j.vibspec.2017.02.003.
27. Dufresne WJB, Rufledt CJ, Marshall CP. Raman spectroscopy of the eight natural carbonate minerals of calcite structure. J Raman Spectrosc. 2018;49:1999–2007. https://doi.org/10.1002/jrs.5481.
28. Sitnikova MA, Do Cabo V, Wall F, Goldmann S. Burbankite and pseudomorphs from the Main Intrusion calcite carbonatite, Lofdal, Namibia: association, mineral composition. Raman Spectrosc Min Mag. 2021;85:496–513. https://doi.org/10.1180/mgm.2021.56.
29. Maiwald M, Sowoidnich K, Sumpf B. Portable shifted excitation Raman difference spectroscopy for on-site soil analysis. J Raman Spectrosc. 2022;53:1560–70. https://doi.org/10.1002/jrs.6400.
30. Frost RL, Williams PA. Raman spectroscopy of some basic chloride containing minerals of lead and copper. Spectrochim Acta A. 2004;60:2071–7. https://doi.org/10.1016/j.saa.2003.11.007.
31. Daniilia S, Minopoulou E. A study of smalt and red lead discolouration in Antiphonitis wall paintings in Cyprus. Appl Phys A. 2009;96:701–11. https://doi.org/10.1007/s00339-009-5163-9.
32. Ma X, Berrie BH. Lead chlorides in paint on a Della Robbia terracotta sculpture. Anal Chem. 2020;92:4935–42. https://doi.org/10.1021/acs.analchem.9b05045.
33. Cui Y, Zheng G, Li J, Li X, Liu Y, Zheng J. Raman spectra and elementseval-uation of a Tang Dynasty Buddha. J Anal Sci. 2011;27:431–4.
34. Zhu T, Wang C, Wang H, Mao Z, Gong M, Wu X, et al. Analysis on the "silvery glaze" of green pottery of Song Dynasty and its form ation mechanism. Chin J Appl Chem. 2007;24:977–81.
35. Zhao Z, Wei S. On glaze color change - formation of "silver glaze" in low temperature lead glazed ceramics. Pop Archaeol. 2020;11:85–8.
36. Zhang W. Analysis on the present situation and restoration countermeasures of soil salinization in northwest region of China. Chem Intermed. 2018;2:26–7.
37. Liu Y, Tong Y, Ma C, Wang B, Zhang X. Current status and regulation measures of soil pH in orchards in Shaanxi region. Shaanxi J Agric Sci. 2019;65:58–61.
38. Yu C, Guo J, Guo W, Liu J, Jian Y. Investigation and analysis of green soil fertility in campus of Xianyang Vocational and Technical College. J Anhui Agri Sci. 2014;42:430–2. https://doi.org/10.13989/j.cnki.0517-6611.2014.17.047.
39. Liu M, Gadikota G. Integrated $CO_2$ capture, conversion, and storage to produce calcium carbonate using an amine looping strategy. Energy Fuels. 2018;33:1722–33. https://doi.org/10.1021/acs.energyfuels.8b02803.
40. Rodrigues A, Gutierrez-Patricio S, Miller AZ, Saiz-Jimenez C, Wiley R, Nunes D, et al. Fungal biodeterioration of stained-glass windows. Int Biodeter Biodeg. 2014;90:152–60. https://doi.org/10.1016/j.ibiod.2014.03.007.
41. Branysova T, Demnerova K, Durovic M, Stiborova H. Microbial biodeterioration of cultural heritage and identification of the active agents over the last two decades. J Cult Herit. 2022;55:245–60. https://doi.org/10.1016/j.culher.2022.03.013.
42. Weaver JL, DePriest PT, Plymale AE, Pearce CI, Arey B, Koestler RJ. Microbial interactions with silicate glasses. Npj Mat Degrada. 2021;5:1–18. https://doi.org/10.1038/s41529-021-00153-w.

## Publisher's Note